HHS Public Access

Author manuscript

Neurobiol Dis. Author manuscript; available in PMC 2023 February 01.

Published in final edited form as:

Neurobiol Dis. 2022 February ; 163: 105608. doi:10.1016/j.nbd.2021.105608.

Myelin and non-myelin debris contribute to foamy macrophage formation after spinal cord injury

Christine B. Ryan[1], **James S. Choi**[1], **Hassan Al-Ali**[1,2,3,4], **Jae K. Lee**[1,*]

[1]University of Miami School of Medicine, Miami Project to Cure Paralysis, Department of Neurological Surgery, Miami, FL 33136

[2]Department of Medicine Katz Division of Nephrology and Hypertension, University of Miami, Miller School of Medicine, Miami, FL.

[3]Peggy and Harold Katz Family Drug Discovery Center, University of Miami, Miller School of Medicine, Miami, FL.

[4]Sylvester Comprehensive Cancer Center, University of Miami, Miller School of Medicine, Miami, FL.

Abstract

Tissue damage after spinal cord injury (SCI) elicits a robust inflammatory cascade that fails to resolve in a timely manner, resulting in impaired wound healing and cellular regeneration. This inflammatory response is partly mediated by infiltrating immune cells, including macrophages. As professional phagocytes, macrophages initially play an important role in debris clearance at the injury site, which would be necessary for proper tissue regeneration. After SCI, most macrophages become filled with lipid droplets due to excessive uptake of lipid debris, assuming a “foamy” phenotype that is associated with a proinflammatory state. Myelin has been assumed to be the main source of lipid that induces foamy macrophage formation after injury given its abundance in the spinal cord. This assumption has led to the widespread use of purified myelin treatment to model foamy macrophage formation *in vitro*. However, the assumption that myelin is necessary for foamy macrophage formation remains untested. To this end, we developed a novel foamy macrophage assay utilizing total spinal cord homogenate to include all sources of lipid present at the injury site. Using the myelin basic protein knockout (MBP KO, i.e., Shiverer) mice that lack myelin, we investigated lipid accumulation in foamy macrophages. Primary macrophages treated with myelin-deficient spinal cord homogenate still formed large lipid droplets typically observed in foamy macrophages, although to a lesser degree than cells

[*]Corresponding author: Jae K. Lee, PhD, University of Miami School of Medicine, Miami Project to Cure Paralysis, Department of Neurological Surgery, 1095 NW 14th Terrace, LPLC 4-19, Miami, FL, 33136, 305-243-2646, JLee22@med.miami.edu.

Christine Ryan: Conceptualization, Methodology, Formal Analysis, Investigation, Visualization, Writing – Original Draft, Writing – Reviewing & Editing, Funding acquisition

James Choi: Conceptualization, Methodology, Formal Analysis, Investigation, Writing – Original Draft

Hassan Al-Ali: Conceptualization, Methodology, Formal Analysis, Writing – Original Draft, Supervision

Jae K. Lee: Conceptualization, Methodology, Investigation, Visualization, Writing – Original Draft, Writing – Reviewing & Editing, Supervision, Project administration, Funding acquisition

treated with normal homogenate. Similarly, MBP KO mice subjected to contusive spinal cord injury also formed foamy macrophages that exhibited reduced lipid content and associated with improved histological outcomes and reduced immune cell infiltration. Therefore, the absence of myelin does not preclude foamy macrophage formation, indicating that myelin is not the only major source of lipid that contributes this pathology, even though myelin may alter certain aspects of its inflammatory profile.

Graphical Abstract

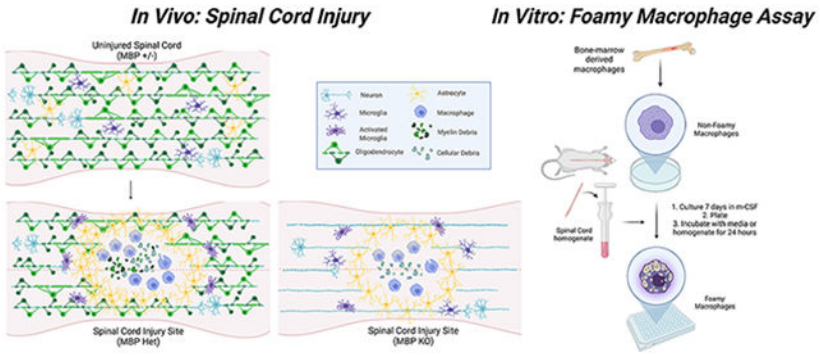

Introduction:

Inflammation is an integral component of the normal wound healing response that restores tissue homeostasis after injury. However, in spinal cord injury (SCI), the wound healing process goes awry, and inflammation does not subside for months or even years (Beck et al., 2010; Fleming et al., 2006). This prolonged inflammatory activation aggravates gliosis, fibrosis, and neuronal cell death at the lesion site, which creates a tissue microenvironment aversive to regeneration. (Beck et al., 2010; Gensel and Zhang, 2015; Hausmann, 2003; Milich et al., 2019; Ren and Young, 2013). Recruitment of leukocytes, including neutrophils and monocytes, potentiates inflammatory signaling through their release of cytokines such as TNF, proteases such as MMP's, as well as production of reactive oxygen and nitrogen species (Donnelly et al., 2011; Fleming et al., 2006; Perrin et al., 2005). Monocytes begin differentiating into macrophages at around 3 days post injury (dpi), with numbers peaking at 7 dpi, and remaining at the lesion site indefinitely (Gensel and Zhang, 2015; Ren et al., 2001; Wang et al., 2015; Zhu et al., 2017). Macrophages interact with almost all cells at the lesion site, mediating important processes such as angiogenesis, gliosis, and scar formation (Kigerl et al., 2009; Milich et al., 2021; Milich et al., 2019; Zhu et al., 2015). However, macrophages have also been shown to contribute to the cellular pathology of SCI by potentiating inflammation and tissue damage and impairing recovery. Multiple studies using models of macrophage depletion have shown improved behavioral and histological outcomes after injury, indicating that macrophages contribute to the maladaptive inflammatory process characterizing the physiological response to SCI (Gris et al., 2004; Popovich et al., 1999; Zhu et al., 2015).

Macrophages are also responsible for clearing away cellular debris through phagocytosis. During this process, however, excessive lipid uptake prompts the formation of lipid-laden

macrophages also known as foamy macrophages, which are found in the human SCI lesion site up to a year after injury (Fleming et al., 2006; Kigerl et al., 2009). Myelin phagocytosis has also been shown to bias macrophage polarization towards a pro-inflammatory phenotype (Ren and Young, 2013; Sun et al., 2010; Wang et al., 2015), although conflicting reports exist in the field of multiple sclerosis research that purport an anti-inflammatory role (Bogie et al., 2013; Boven et al., 2006). In addition to modulating the inflammatory response, myelin-treated foamy macrophages have also been shown to exhibit impaired migratory capacity in a scratch wound healing assay, which is consistent with the persistence of macrophages and failure to emigrate from the lesion site in both SCI and atherosclerosis (Nguyen et al., 2018; Wang et al., 2015).

Considering the abundance of myelin debris post-SCI, and that macrophages exhibit a predominantly pro-inflammatory phenotype long-term in the injured spinal cord, these data are all consistent with the role of foamy macrophages as perpetrators of pathological inflammation after SCI (Kigerl et al., 2009; Kroner et al., 2014; Wang et al., 2015). Stimulating lipid efflux with AdipoRon, an agonist for the atheroprotective hormone adiponectin, resulted in decreased lipid accumulation at the injury site, alleviation of post-SCI inflammation and restoration of motor function (Zhou et al., 2019). Genetic deletion of the scavenger receptor CD36, which has been implicated in foamy macrophage formation in atherosclerosis, decreased lipid droplet number, reduced lesion size, and improved locomotion scores after SCI (Myers et al., 2014; Zhu et al., 2017). These studies cast foam cells as an attractive target for therapeutic intervention in the context of SCI and macrophage-mediated inflammation.

Previous studies investigating foamy macrophage formation *in vitro* commonly utilized purified myelin treatment to induce this phenotype. Conflicting reports of the effect of myelin on macrophage phenotype and polarization arise from issues with experimental design. Such discrepancies include technical challenges and variability in myelin purification, as well as differences in treatment paradigms (Kopper and Gensel, 2018). To elucidate the effect of myelin on the inflammatory status of macrophages, different studies utilize different pro- and/or anti-inflammatory cues either before or alongside myelin treatment, measuring downstream alterations in expression of inflammatory mediators to substantiate their conclusions. The type of inflammatory priming (pro- or anti-inflammatory) and the order of treatment relative to myelin (pre- or co-treatment) produces divergent effects, making it difficult to gain insights into the nature of myelin-treated macrophages (Bogie et al., 2013; Boven et al., 2006). For example, when macrophages were pre-treated with anti-inflammatory polarizing stimuli before myelin treatment, increased pro-inflammatory and decreased anti-inflammatory markers was observed compared to stimulated cells not treated with myelin (Siddiqui et al., 2016; Wang et al., 2015). Conversely, pre-treatment or co-treatment of myelin with pro-inflammatory stimuli such as LPS produced divergent effects on inflammatory response, with reports of both increase and decrease in pro-inflammatory characteristics relative to stimulated cells not treated with myelin (Kopper et al., 2021; Kroner et al., 2014; Sun et al., 2010; van der Laan et al., 1996). Post-treating macrophages with LPS after myelin, however, produced a dampened inflammatory response relative to LPS alone, again highlighting the challenges in studying foamy macrophages in this manner (Bogie et al., 2013; Boven et al., 2006).

Furthermore, implicit in the use of purified myelin is the underlying assumption that myelin itself is the only or the most important source of lipid debris contributing to foamy macrophage formation. An assay that appropriately models the inflammatory environment and the lipid debris present at the injury site will be instrumental in clarifying the role of foamy macrophages in SCI. To address this issue, we treated primary bone-marrow derived macrophages (BMDMs) with total spinal cord homogenate which is more representative of the cellular debris and inflammatory cues at the injury site. Furthermore, to directly test the contribution of myelin to foamy macrophage formation after SCI, we used this assay on BMDMs treated with myelin-deficient MBP KO homogenate. We also performed contusive SCI on MBP KO mice to assess the contribution of myelin to foamy macrophage formation *in vivo*. Our data show that while myelin contributes to their lipid content, foamy macrophages can form without myelin both *in vitro* and *in vivo*, and reduction in foamy macrophages at the lesion site alters the histopathology and immune profile of the injury site.

Methods:

Foamy macrophage assay:

Bone marrow-derived macrophages were isolated from 8-12-week-old male and female C57BL/6J mice (Jackson Labs, Stock 000664). Briefly, femur and tibia bones were dissected, and bone marrow flushed out with RPMI using a 25-gauge needle. Single cell suspension was obtained by passing the bone marrow through a 70μM strainer (VWR Cat# 21008-952) and then red blood cells were lysed using RBC lysis buffer (155 mM NH4Cl, 10 mM KHCO3, 0.09 mM Na4-EDTA). Cells were cultured in a T75 flask (VWR Cat# 82050-856) in media containing 20% L929 fibroblast-conditioned-media, 10% Fetal Bovine Serum, 50 μM Beta-mercaptoethanol and antibiotic/antimycotic in RPMI 1640 (ATCC modification: 4.5 g/L D-Glucose, 2.4 g/L HEPES, 1.5 g/L Sodium Bicarbonate, 110 mg/L Sodium Pyruvate, supplemented with L-glutamine). The day after isolation, cells were washed with HBSS to remove any floating cells and media changed, with an additional media change two days thereafter. After five days in culture, cells were washed, trypsinized and plated at 60,000 cells per well in a 96-well plate (with micro-clear bottom, Greiner) at 100μL per well.

For homogenate preparation, 8-12-week-old male and female C57BL/6 mice were perfused with ice cold PBS, spinal cords dissected, and meninges removed to avoid fibroblast contamination in culture. Multiple cords were pooled together, diced with a razor blade, and then separated into aliquots and frozen. On the day that macrophages needed to be treated with homogenate, cords were thawed, weighed, and homogenized with a Dounce homogenizer in cell culture media to produce a 10X mixture of 100 mg cord/mL media (10% weight/volume). To homogenize, cord was transferred to the Dounce grinder and appropriate volume of complete media was added. Both A and B pestles were used sequentially for 15 strokes each, ensuring no bubbles were generated in the homogenate. 10 μL of this mixture was directly added to each well with vehicle/compounds for final concentration of 10 mg/mL or 1% w/v in the well. After 24 hours incubation, homogenate and media were removed, and cells were washed gently three times with HBSS (no calcium,

no magnesium, no phenol red, Gibco, Catalog number: 14175095) to ensure complete removal of residual homogenate without disrupting the cell monolayer.

After complete removal of homogenate, cells were fixed with 4% paraformaldehyde for 15 minutes at room temperature. We then stained intracellular lipids with a Nile Red solution (100μg/mL diluted in PBS, Invitrogen Nile Red, ThermoFisher Catalog No. N1142) for 15 minutes at room temperature, followed by DAPI (1:10,000 of 5 mg/mL stock, ThermoFisher Catalog No. D1306) and CellMask Deep Red staining (1:5,000, ThermoFisher Catalog No. C10046) diluted in PBS to visualize the nuclei and cell bodies respectively. Solvatochromic dye Nile Red was used to specifically stain neutral lipid droplets in the green channel, given its fluorescence emission blue-shift in non-polar environments. Images were acquired using the Opera High Content Imaging system (PerkinElmer) at 25 images/well.

Images were uploaded onto the Columbus software (PerkinElmer) as FLEX files. Analysis first identified DAPI-positive nuclei using “Method B” and used CellMask to outline “Cytoplasm” area using “Method B”. Only the identified cells between 150-2000 μm^2 and a CellMask Intensity > 75 were selected for additional analysis. Lipid droplets were detected in the “cytoplasm” region (CellMask region with subtracted DAPI area) using “Method C” and only spots with Spot Contrast > 0.1, Spot to Region Intensity > 0.5, and Uncorrected Spot Peak Intensity > 400 were chosen for additional analysis. Of the spots selected, mean fluorescence intensity per cell and average spot number per cell was calculated. At each step, proper nuclei and cell membrane segmentation was confirmed visually, as well as proper Spot identification, before continuing with analysis. Due to fluctuations in staining and imaging, these parameters required slight modifications to ensure proper identification of signal while discarding artifacts.

The Z’-factor represents the suitability of a given assay for high-content screening by measuring the amount of separation between the positive and negative control populations while also accounting for their variability. Z’ values were calculated with the following equation:

$$Z' = 1 - \frac{3\sigma_p + 3\sigma_n}{|\mu_p - \mu_n|}$$

where μ (mean) and σ (standard deviation) and p subscript refers to positive control (or the 1% homogenate-treated condition), and n subscript refers to negative control (or the media-treated condition). A Z’ factor in the range of 0.5-1.0 is considered excellent. Hill slope, EC50, and R-square values for goodness-of-fit were calculated automatically using the nonlinear regression analysis function with variable slope (four parameters). Least squares ordinary fit was used for fitting method, with constraint that EC50 must be greater than 0. Calculations performed in GraphPad Prism version 7.05 for Windows (GraphPad Software, La Jolla California USA):

$$Y = \frac{Bottom + (X^{Hill\ slope})(Top - Bottom)}{(X^{Hill\ slope} + EC50^{Hill\ slope})}$$

Where EC50 is the homogenate concentration that gives response halfway between the Top (upper limit of Y) and Bottom (lower limit of Y). Hill slope represents the steepness of the curve, with Hill slope of 1.0 representing a perfectly linear relationship.

Gene expression analysis:

For quantitative polymerase chain reaction (qPCR) analysis, cells were washed and resuspended in RLT Lysis Buffer plus beta-mercaptoethanol (10 μL per 1 mL of buffer, Sigma Catalog: M6250). RNA was extracted using the RNeasy Micro Kit (Qiagen) according to manufacturer instructions. RNA quantity was measured using a NanoDrop 1000, reverse transcribed into cDNA using iSCRIPT kit using a Corbett Research RG 3000 thermal cycler (Qiagen, Valencia, CA). cDNA was used for qPCR on the QuantStudio 3 Real-Time PCR System (Applied Biosystems) using SYBR Green Fast Master Mix (Applied Biosystems, Catalog 4385612) and primers targeting intron-spanning mRNA sequences. Fold-change in gene expression relative to untreated controls was normalized to beta-actin and quantified using the ddCT method.

Spinal Cord Injury Surgeries:

8-10 weeks old female MBP Het and MBP KO (Jackson Stock 001428) mice received contusive spinal cord injuries as previously described (Zhu et al., 2017; Zhu et al., 2015). As recently reviewed by Stewart et al. (2020), the presence of sex as a biological variable is a relevant concern for spinal cord injury studies. However, these differences tend to be outcome-specific. For the purpose of the present study, our aim was to assess lipid content in foamy macrophages and other aspects of lesion pathology. Unpublished images of the male and female injury site at 7 dpi demonstrate that foamy macrophages form in both male and female lesion site. Additionally, we utilized both male and female animals in our in vitro foamy macrophage experiments and did not observe any phenotypic differences. Briefly, mice were anesthetized via intraperitoneal injection with a ketamine/xylazine cocktail (100mg/15mg/kg i.p.), followed by a T8 laminectomy. The spinal column was stabilized using clamps and the exposed T8 spinal cord was placed directly below the Infinite Horizon impactor device (Precision Systems Instrumentation, LLC), and mice received a moderate (65 kdyne) T8 contusion. Mice received a single dose of extended-release buprenorphine (Buprenex-SR, 1mg/kg, s.c.), followed by 3 days of gentamycin (5 mg/kg, s.c.) once daily and 7 days of Lactated Ringer's solution (1 mL, s.c.) twice daily. Manual bladder expression was performed twice daily for the duration of the experiment. All animal procedures adhered to University of Miami IACUC and NIH guidelines. Normal attrition rate for female mice after surgery is approximately 10%, although concerns regarding MBP KO viability after injury informed our decision to utilize a greater number of MBP KO animals in initial in vivo studies (7 dpi: n=4 MBP Het; n=7 MBP KO, no deaths). When we did not observe a marked increase in death in MBP after injury, we used equal numbers in both groups upon power analysis in future studies (28 dpi: n=7 MBP Het; n=6 MBP KO after loss of n=1 MBP KO).

Immunohistochemistry:

At the end of the experiment, mice were anesthetized with avertin (250mg/kg, i.p) and euthanized by transcardial perfusion with cold 4% paraformaldehyde (PFA). Spinal cord

was dissected and postfixed for 2 hours and then cryoprotected in 30% sucrose solution in PBS all at 4°C. 8mm segment of the spinal cord centered at the injury site was embedded in OCT compound (Tissue-Tek) and cryosectioned stepwise in serial sagittal sections (16μm) to produce a group of slides that each represents the entire width of the injury site. Slides were stored at −20°C until further use. For immunohistochemical staining, slides were dried at room temperature and then washed with PBS before permeabilizing and blocking (5% normal goat serum in PBS-T, PBS in 0.3% Triton-X) for 1 hour at room temperature. Slides were stained overnight at 4°C with antibodies diluted in blocking buffer (5% NGS in PBS-T). Antibodies used include rat anti-mouse CD11b (1:200, Biorad Ref MCA74GA), chicken anti-mouse GFAP (1:500, Abcam, ab4674), and biotinylated mouse-NeuN antibody (1:400, Millipore, MAB377B). After primary antibody incubation, slides were washed with PBS and then incubated with Alexa-Fluor antibodies (1:500 in PBS-T) or streptavidin-tagged Alexa-Fluor antibodies (1:500 in PBS-T) for 1 hour at room temperature, followed by additional PBS washes. For Oil Red O staining, 0.5% Oil Red O (Sigma, O0625) solution dissolved in propylene glycol (Sigma, P4347) was prewarmed to 60 °C. Slides were pre-treated with 100% propylene glycol for 5 minutes, followed by immersion in Oil Red O solution for 20 minutes. Oil Red O was removed, and slides were post-treated for 5 minutes in an 85% propylene glycol solution diluted in distilled water. Slides were washed with PBS and then incubated with DAPI (1:10,000 of 5 mg/mL stock, ThermoFisher Catalog No. D1306). Images were taken using Nikon (Melville, NY) Eclipse Ti fluorescent microscope with a 20x objective, and experimenters were blinded to the animal identities using a random number generator. Oil Red O fluorescence and area fraction were measured using ImageJ after background subtraction. GFAP-negative lesion area was quantified using manual measurement tool on ImageJ as a percentage of spared GFAP-positive neural tissue. Representative confocal images were taken using the Andor Dragon Confocal Imaging System (Oxford Instruments) with 10X objective for overview images and 63X for high-magnification insets.

Flow Cytometry:

For flow cytometric analysis, injured mice were anesthetized with avertin and euthanized by perfusion with ice cold PBS at 7 dpi. Meninges were removed and an 8mm section of the spinal cord was dissected. Spleen samples were also collected for controls. Samples were mechanically homogenized against a 70μm cell strainer and washed through with HBSS (no calcium, no magnesium, no phenol red, Gibco, Catalog number: 14175095). Samples were spun down in swinging-basket centrifuge for 10 minutes at 300g at 4°C and resuspended in 90μL MACS Buffer (0.5% BSA in HBSS w/o Ca2+/Mg2+). Myelin was removed using Miltenyi Myelin Removal Beads II (Cat #: 130-096-733) and LS Miltenyi MACS Magnetic Bead Columns (Cat#: 130-042-401), according to manufacturer's instruction. Cells were then washed with PBS, centrifuged 10 minutes at 300g and resuspended in Zombie Aqua Viability dye (1:500, Biolegend Cat. 423101) in PBS for 15 minutes at 4°C. Cells were then washed with FACS buffer (1% BSA + 0.05% sodium azide in HBSS w/o Ca2+/Mg2+) and resuspended in TruStain fcX anti-mouse CD16/36 blocking solution (1:100, Biolegend Cat. 101319) in FACS, 10 min at room temperature. Surface antibodies were then added to cell mixtures: APC/Cy7-CD45 (1:200, Biolegend Cat.103116), APC-cd11b (1:200, Biolegend Cat. 101212), PerCP/Cy5.5 Ly6G (1:200, Biolegend Cat. 127616), PE B220

(1:500, eBiosciences/ThermoFisher, Cat. 11-0452-81), and PE/Cy7 CD3 (1:200, Biolegend, 100219) and cells incubated for 15 minutes at 4°C. Cells were washed with PBS and then stained with BODIPY 493/504 (1:100, ThermoFisher Cat. D3922) in PBS for 20 min at room temperature. Cells were washed again, each sample resuspended in 250μL FACS buffer in F-bottom 96 well plates, and 10μL of 123 eBeads Counting Beads added to each sample (ThermoFischer Scientific Cat #: 01-1234-42). Cells were kept at 4°C until analysis on a Cytoflex Flow Cytometer (Beckman Coulter). Single color compensation controls from spleen samples were used and macrophage/microglia gating verified using spleen samples and uninjured cord rostral/caudal to injury site. Cells were then washed twice and stored in 0.5% PFA until read on flow cytometer. BODIPY was validated *in vivo* by comparing BODIPY signal in macrophages at 3 dpi (n=4) when there are much fewer foam cells, and at 7 dpi (n=4) when there is a substantial foam cell population. Four C57BL/6J mice per time point were subjected to T8 contusion, staggered four days apart so perfusion and flow analysis could be done on same day. Similarly, because our interest was in characterizing peripheral leukocyte populations, the use of sham controls where these populations are absent was not included.

Results:

Previous studies that have investigated macrophage phagocytosis after CNS injury commonly utilize purified myelin treatment *in vitro*. To better represent all the exogenous lipid sources present at the injury site, we developed a novel *in vitro* assay wherein we generate foamy macrophages from bone-marrow-derived macrophages (BMDMs) treated with spinal cord homogenate rather than purified myelin. Macrophages were treated for 24 hours at increasing concentrations of total homogenate (0.01%, 0.1%, 0.5%, 1.0%, 2.0% w/v) (Figure 1 A, B). After washing and fixation, macrophage lipid droplets were stained with lipid soluble dye. Comparison of lipid dyes Nile Red, BODIPY 493/503, and Oil Red O was assessed over the range of homogenate concentrations mentioned above. Z-prime factor (Z') calculations between the positive (1% homogenate) and negative (media) controls and nonlinear regression analysis of the homogenate dose response curve were performed. Z' evaluates the separation of the data variability band between positive and negative control dataset, thereby assessing the suitability of the assay for screening purposes. Z' between 0.5-1 is considered excellent with 1 being the highest score (see methods). Hill slope derived from the nonlinear regression analysis describes the linearity of the dose response curve, with a perfectly linear Hill slope=1.0. Analysis revealed Nile Red as the most suitable for high content analysis (Z'= 0.693), and the one with the best linear range (Hill slope= 1.029), compared to BODIPY (Z'=0.684; Hill slope=2.40) and Oil Red O (Z' =0.313, Hill slope=1.005) (Supplemental Figure 1). Nile Red is highly solvatochromic and undergoes large fluorescence enhancement and emission blue-shift in nonpolar environments, thereby emitting green (instead of red) light only when present inside lipid droplets. This results in better signal to noise ratio and likely underlies the improved assay sensitivity with Nile Red. Using a high content screening platform, we imaged and quantified multiple parameters to assess lipid accumulation in foamy macrophages including lipid droplet intensity and number. Cell and nucleus boundaries were detected, and individual lipid droplets were identified in the cytoplasm (Figure 1C). To determine which parameter was best for assay

development, we calculated the Z' factor for both spot intensity and spot number. Treatment at increasing concentrations of homogenate produced a concentration-dependent response in both lipid droplet spot intensity (Figure 1D, E, Z'=0.70) and number (Figure 1G, H, Z'=0.87) with spot number reaching a plateau at a lower concentration (Figure 1 D, G). Analysis of Hill slope (spot intensity Hill Slope=1.06, spot number Hill Slope=1.31) and goodness-of-fit (spot intensity R-square=0.921, spot number R-square=0.874) from a four-parameter nonlinear regression fit revealed spot intensity as the superior readout due to its linearity over a wider dynamic range (Figure 1F, I). Previous work demonstrated that genetic deletion of the lipid importer, CD36, reduced lipid content and improved histological and behavioral outcomes after spinal cord injury (Myers et al., 2014; Zhu et al., 2017). As a proof-of-concept, we performed the foamy macrophage assay on CD36 knockout (KO) and wildtype (WT) BMDMs (Figure 2A, B). CD36 KO macrophages displayed significantly reduced lipid droplet fluorescence compared to WT macrophages, demonstrating the utility and biological relevance of the *in vitro* assay in modeling foamy macrophage formation after SCI.

To directly test the contribution of myelin to foam cell formation, we utilized the Shiverer mouse model that lacks central nervous system (CNS) myelin due to a mutation in myelin basic protein (MBP). We measured lipid droplet spot intensity in WT macrophages treated with 0.01%, 0.1%, and 1% (w/v) MBP heterozygote (Het) and MBP KO spinal cord homogenate (Figure 3 A, B). MBP Het mice contain one functional copy of the MBP gene that is sufficient to generate normal compact myelin, which allowed for the use of littermate controls of the same genetic background. It should be noted that the total amount of myelin in hetereozygous littermates is approximately 35% lower than wildtypes (Cammer et al., 1984). Lipid droplets still formed in cells treated with the MBP KO homogenate despite the absence of myelin (Figure 3B). Macrophages treated with MBP KO homogenate exhibited a reduction in spot intensity compared to cells treated with 1% MBP Het homogenate (Figure 3C). qPCR analysis of foamy macrophages generated from MBP KO homogenate also exhibited significantly reduced expression of pro-inflammatory cytokines *Ccl2* and *Cxcl10*, suggesting that increased lipid content from myelin and/or myelin-specific factors potentiate the inflammatory response in foamy macrophages (Figure 3D). To address concerns about potential differences in basal level of inflammatory cytokines between the two types of MBP homogenates, we quantified expression of several pro-inflammatory cytokines in uninjured MBP Het and MBP KO cords. qPCR analysis did not reveal any differences in baseline inflammatory activation (Supplemental Figure 2C).

To determine the contribution of myelin to foamy macrophage formation *in vivo*, we subjected MBP KO mice and their MBP Het littermate controls to contusive mid-thoracic spinal cord injury and assessed histology at 7 and 28 days post injury (dpi) (Figure 4A, B). We used a neutral lipid dye Oil Red O (ORO) combined with CD11b immunohistochemistry to visualize lipid-laden CD11b-positive cells at the injury site. Foamy CD11b-positive cells still formed in the KO mice, recapitulating our *in vitro* findings, and underscoring the importance of considering all physiologically relevant sources of lipids when modeling foamy macrophage formation. Quantification of the lesion site indicated decreased ORO staining intensity and area coverage in the MBP KO mice (Figure 4C, D). The decreased ORO signal was observed at both 7 dpi when lipid droplets were more diffusely dispersed

across the injury site, and 28 dpi when lipid droplets consolidated to the lesion core. These results demonstrate that neutral lipid droplets can form at the injury site in the absence of myelin.

During the course of ORO quantifications, we observed significantly less CD11b-positive macrophages at the MBP KO injury site as compared to Het controls (Figure 4A, B), which raised the possibility that reduced ORO signal could have been due to decreased macrophage number. Because histology alone cannot distinguish which CD11b+ subpopulations are responsible for this effect (i.e. microglia, macrophages, neutrophils), we confirmed our histological observations using flow cytometric analysis of MBP Het and MBP KO 7 dpi injury site (Figure 5A-C), which showed significantly reduced macrophages at the MBP KO injury site both in number (Figure 5D) and percentage of total CD45-positive leukocytes (Figure 5E). MBP KO mice also exhibited significant reductions in the number of other types of leukocytes including T cells and B cells (Figure 5G). However, when normalized to percentage of all CD45+ leukocytes, these differences were not statistically significant suggesting an overall reduction in lymphocytes rather than specific populations (Figure 5H). To ensure there was no global deficit in peripheral leukocytes in MBP KO mice, analysis of spleens from MBP Het and MBP KO SCI mice revealed no differences in leukocyte number indicating that the decrease in macrophages at the MBP KO injury site does not reflect peripheral deficits in leukocyte pools (Figure 5F, I). Taken together, our data indicate that there is a significant reduction in leukocyte infiltration (especially macrophages) after SCI in MBP KO mice.

To address whether the reduced ORO signal in MBP KO mice was due to reduced macrophage infiltration, we performed flow cytometry on the 3 and 7 dpi injury sites by staining foamy macrophages with BODIPY, a neutral lipid stain compatible with the flow cytometry protocol due to its excitation/emission fluorescence properties. The BODIPY stain was validated for its ability to label foamy macrophages *in vivo* by demonstrating the absence of a BODIPY-hi macrophage population in the spleen and spinal cord tissue rostral and caudal to the injury site, but their increasing presence from 3 to 7 dpi at the injury site (Figure 6A). When normalized to the number of macrophages, the percentage of BODIPY-hi foamy macrophages in MBP KO injury site were about half that of foamy macrophages in MBP Het mice (Figure 6B), which is consistent with our ORO histological quantifications. Together, these results confirm that myelin contributes to foamy macrophage formation after SCI, but is not the only exogenous lipid source driving this process.

To ensure that the reduction in lipid content at the MBP KO injury site was not the result of some deficit in debris phagocytosis or lipid processing in macrophages, we cultured MBP Het and MBP KO BMDMs and treated them with wildtype spinal cord homogenate. Both the MBP Het and KO foamy macrophages exhibited similar concentration-dependent increases in lipid droplet intensity, demonstrating that BMDMs in MBP KO and Het mice do not differ in their ability to become foamy macrophages (Supp Figure 2A, B)

To understand the pathological consequences of reducing foamy macrophage formation after injury, we assessed the lesion histopathology in the MBP Het and KO mice. We found that reduced ORO signal at 7 and 28 dpi was associated with a significant reduction in lesion size

as defined by GFAP-negative area (Figure 7). Due to severe motor impairments in the MBP KO mice at baseline, accurate assessment of behavioral recovery through tests such as the Basso Mouse Scale was not feasible. Reduction in lesion size in the KO mice indicates that loss of myelin in the MBP KO mice alters lesion pathology. Additional studies are needed to directly attribute this effect to the observed reduction in foamy macrophages. Thus, based on our *in vitro* and *in vivo* data, we conclude that foamy macrophages can form without myelin debris, albeit at decreased levels, and that both myelin and non-myelin sources of lipids must be considered when investigating contribution of foamy macrophages to CNS pathobiology.

Discussion:

In this study, we used MBP KO mice to directly test the contribution of myelin to foamy macrophage formation both *in vitro* and *in vivo*. Our results demonstrate that while myelin certainly contributes to lipid droplet accumulation in foamy macrophages, non-myelin debris are also major contributors to foamy macrophage formation. In fact, our analyses suggest that about half of neutral lipid content in foamy macrophages are from non-myelin sources. The novel foamy macrophage assay developed in this paper addresses an unmet need in the field to model and understand the contribution of foamy macrophages to CNS pathology.

The current paradigm for modeling foamy macrophages *in vitro* involves the use of purified myelin, which can be fraught with multiple shortcomings (reviewed in Kopper and Gensel (2018)]. Some studies treat with myelin alone, reporting a variety of pro-inflammatory and anti-inflammatory effects (Kroner et al., 2014; van der Laan et al., 1996; van Rossum et al., 2008; Wang et al., 2015). Other studies pre-treat macrophages with myelin and report a dampened inflammatory or anti-inflammatory response to subsequent stimulation (Bogie et al., 2013; Boven et al., 2006). Alternatively, pre-treatment with inflammatory stimuli followed by myelin potentiates the M1 phenotype (Siddiqui et al., 2016; Van Broeckhoven et al., 2021). Co-treating myelin with pro-inflammatory signals induces an initial M1-like response, followed by a subsequent conversion to an anti-inflammatory phenotype (Liu et al., 2006). Another permutation of this protocol compares the effect of pre-treating with pro-inflammatory stimulus, followed by removal or retaining of this stimulus upon myelin treatment (Kroner et al., 2014). Removal of the stimulus upon myelin introduction produced an M2-like profile, whereas co-treating myelin with the inflammatory stimulus enhanced the M1-like response (Kopper et al., 2021; Kroner et al., 2014). These results are consistent with recent work demonstrating that the effects of lipid phagocytosis on macrophages depend on the macrophage activation state. (Kopper et al., 2021). Technical challenges related to myelin purification represents another contributor to variability. The classic protocol for myelin purification utilizes an isotonic sucrose gradient that separates myelin vesicles via density gradient centrifugation into discrete layers of varying densities (Arstila et al., 1970; Bellini et al., 1986; Erwig et al., 2019; Rumsby et al., 1970). This isolation technique must also be followed by appropriate quality control measures to ensure purity of myelin content such as CNPase colorimetric assay (Larocca and Norton, 2007; Rumsby et al., 1970).

Together, differences in experimental protocol and technical concerns demonstrate the need for standardization across studies. The use of uninjured spinal cord homogenate to induce lipid droplet accumulation represents a novel yet simple solution to address some of these

concerns since it requires minimal processing. Although using homogenate from the injury site would be the ideal mimic of the lesion microenvironment, the number of injury sites required to generate enough homogenate, and the variability across SCI surgeries raises animal use and reproducibility issues. However, total spinal cord homogenate provides most sources of biologically relevant lipids beyond myelin, and the inflammatory cues such as DAMP'S (Damage Associated Molecular Patterns), cytokines and apoptotic cells to approximate the inflammatory milieu at the injury site. One potential criticism of the proposed assay pertains to concerns of variability across homogenate preparations. To address this issue, performing large scale isolation of fresh spinal cord in a single session that can be pooled together permits the use of similar aliquots of fresh frozen spinal cord to homogenize when necessary. It is also important to note the myelin isolation and purification protocols are technically more challenging than homogenate preparation while also posing greater risk to reproducibility across batches and different personnel.

The controversy over the effect of myelin *in vitro* calls into question the contribution of myelin phagocytosis on macrophage polarization after CNS injury *in vivo*. The time course of the appearance of foamy macrophages at the injury site at 7 dpi corresponds to observed pro-inflammatory macrophage polarization state after SCI (Kigerl et al., 2009; Wang et al., 2015; Zhu et al., 2017). Accordingly, dampening excessive lipid phagocytosis through knockout or inhibition of scavenger receptors such as CD36 resulted in improved motor recovery and histopathology after SCI (Kong et al., 2020; Myers et al., 2014; Zhu et al., 2017). However, work in other disease models such as multiple sclerosis has shown that macrophages in the center of demyelinated regions co-localize with anti-inflammatory markers, suggesting a pro-regenerative phenotype. (Bogie et al., 2013; Boven et al., 2006; Liu et al., 2006). Our results demonstrate that myelin only represents about half of the physiological lipid sources contributing to foamy macrophage formation, and that macrophages treated with myelin-deficient homogenate express lower levels of several but not all pro-inflammatory cytokines (Figure 2). This indicates the presence of both myelin-dependent and myelin-independent phenomena responsible for uniquely modulating the foamy macrophage inflammatory signature and its subsequent role in shaping the pathophysiology of the SCI lesion site.

A confound in the MBP *in vivo* experiments pertains to the significantly lower number of macrophages present in the MBP KO mice injury site. It remains unknown whether the reduced macrophage population at the injury was the cause or the product of reduced foamy macrophages at the injury site and subsequent attenuation of inflammatory activation and release of chemotactic cues. The reason for reduced macrophage number in the MBP KO mice may be due to absence of myelin debris, which can act as a chemotactic cue initiating the robust infiltration of infiltrating leukocytes after injury (Sun et al., 2010). Our flow cytometry experiments addressed aspects of this concern by normalizing for differences in total macrophage number when quantifying BODIPY fluorescence, which demonstrated a decrease in foamy macrophages at the MBP KO injury site. Due to severe motor deficits in the uninjured MBP KO mice at baseline, proper assessment of functional motor recovery after injury was not possible, and it remains to be seen if the decrease in lipid droplet intensity, lesion size, and immune cell population observed in the MBP KO mice manifested in behavioral improvements (Bird et al., 1978; Matthieu et al., 1981; Nagaike et al., 1982).

Another question arising from our studies relates to the source of lipid debris driving lipid droplet formation in macrophages in the absence of myelin *in vitro* and *in vivo*. Previous work has characterized the lipid content of Shiverer mice compared to controls, demonstrating that certain lipid classes, namely galactolipids (cerebrosides), represent the main lipid class deficient in the Shiverer cortex (Bird et al., 1978). Other lipids, such as phospholipids and gangliosides, are present in the Shiverer CNS in equal amounts as normally myelinated controls and are likely from the membranes of its cellular constituents (Bird et al., 1978). The potential for myelin-specific effects (versus lipid content) in shaping the foamy macrophage phenotype may be attributed to the presence of myelin-related lipids (i.e. galactolipids) or protein expression (i.e. MBP itself) . Such potential myelin-specific effects include the decreased expression of CCL2 and CXCL10 in foamy macrophages treated with MBP KO homogenate rather than or in addition to decreased lipid content. Similarly, the reduced infiltration of immune cells in the MBP KO could be a result of myelin-specific alterations to the inflammatory profile. Discerning whether there are myelin-specific effects on the foamy macrophage phenotype is complicated by the ability to normalize for total lipid in the MBP Het vs MBP KO homogenates. Normalizing lipid content by lipid droplet fluorescence requires a near 5-fold increase in MBP KO homogenate (Supp Figure 2 D, E) which results in higher protein content and higher concentration of other molecular cues present in the homogenate. When normalizing MBP Het and KO homogenates by weight per unit volume (%), there are no differences in total protein content as assessed by BSA (data not shown) and therefore represents the closest solution to the issue of normalization across these homogenates.

In summary, our data demonstrate that myelin is not the sole source of lipid driving foamy macrophage formation *in vitro* and *in vivo*. We developed a novel *in vitro* foamy macrophage assay suitable for high content analysis that utilizes total spinal cord homogenate to better model the SCI lesion microenvironment. Together with *in vivo* studies, this foamy macrophage assay provides a platform for future studies to mechanistically investigate lipid-laden foam cells after spinal cord injury, and to identify potential drug targets that can be translated into therapeutics for treating SCI.

Supplementary Material

Refer to Web version on PubMed Central for supplementary material.

Acknowledgments:

Authors would like to thank Kaila Hundley for assistance in histology quantifications, Shaffiat Karmally for assistance with behavioral testing and animal care. We thank Yan Shi at the Miami Project to Cure Paralysis Imaging Core for assistance with Opera imaging and analysis We thank Dr. Oliver Umland at the Diabetes Research Institute Flow Cytometry Core for assistance with flow experiments and Drs. Javier Varona-Santos and Alexis Sloan for assistance with Opera imaging. Graphical abstract created with BioRender.com

Funding Sources:

This study was funded by The Miami Project to Cure Paralysis, The Buoniconti Fund, NINDS R01NS081040, NINDS F31NS115225

Abbreviations:

SCI	spinal cord injury
dpi	days post injury
MBP	myelin basic protein
KO	knockout
Het	heterozygote
TNF	Tumor Necrosis Factor
MMP	matrix metalloprotease
BMDMs	bone-marrow-derived macrophages
PBS	phosphate buffered saline
HBSS	Hanks Balanced Salt Solution
i.p.	intraperitoneal
s.c.	subcutaneous
CNS	central nervous system
qPCR	quantitative polymerase chain reaction
ORO	Oil Red O
DAMP	Damage Associated Molecular Pattern
HCS	High Content Screening

References:

Arstila A, et al. , 1970. Critical re-evaluation of the purification methods of myelin by using quantitative morphometric and chemical analyses. Acta Neurol Scand. 46, 229–30. [PubMed: 5457831]

Beck KD, et al. , 2010. Quantitative analysis of cellular inflammation after traumatic spinal cord injury: evidence for a multiphasic inflammatory response in the acute to chronic environment. Brain. 133, 433–47. [PubMed: 20085927]

Bellini T, et al. , 1986. A rapid method for purification of myelin basic protein. J Neurochem. 46, 1644–6. [PubMed: 2420937]

Bird TD, et al. , 1978. Brain lipid composition of the shiverer mouse: (genetic defect in myelin development). J Neurochem. 31, 387–91. [PubMed: 671037]

Bogie JF, et al. , 2013. Myelin alters the inflammatory phenotype of macrophages by activating PPARs. Acta Neuropathol Commun. 1, 43. [PubMed: 24252308]

Boven LA, et al. , 2006. Myelin-laden macrophages are anti-inflammatory, consistent with foam cells in multiple sclerosis. Brain. 129, 517–26. [PubMed: 16364958]

Cammer W, et al. , 1984. Biochemical abnormalities in spinal cord myelin and CNS homogenates in heterozygotes affected by the shiverer mutation. J Neurochem. 42, 1372–8. [PubMed: 6200571]

Donnelly DJ, et al. , 2011. Deficient CX3CR1 signaling promotes recovery after mouse spinal cord injury by limiting the recruitment and activation of Ly6Clo/iNOS+ macrophages. J Neurosci. 31, 9910–22. [PubMed: 21734283]

Erwig MS, et al. , 2019. Myelin: Methods for Purification and Proteome Analysis. Methods Mol Biol. 1936, 37–63. [PubMed: 30820892]

Fleming JC, et al. , 2006. The cellular inflammatory response in human spinal cords after injury. Brain. 129, 3249–69. [PubMed: 17071951]

Gensel JC, Zhang B, 2015. Macrophage activation and its role in repair and pathology after spinal cord injury. Brain Res. 1619, 1–11. [PubMed: 25578260]

Gris D, et al. , 2004. Transient blockade of the CD11d/CD18 integrin reduces secondary damage after spinal cord injury, improving sensory, autonomic, and motor function. J Neurosci. 24, 4043–51. [PubMed: 15102919]

Hausmann ON, 2003. Post-traumatic inflammation following spinal cord injury. Spinal Cord. 41, 369–78. [PubMed: 12815368]

Kigerl KA, et al. , 2009. Identification of two distinct macrophage subsets with divergent effects causing either neurotoxicity or regeneration in the injured mouse spinal cord. J Neurosci. 29, 13435–44. [PubMed: 19864556]

Kong FQ, et al. , 2020. Macrophage MSR1 promotes the formation of foamy macrophage and neuronal apoptosis after spinal cord injury. J Neuroinflammation. 17, 62. [PubMed: 32066456]

Kopper TJ, Gensel JC, 2018. Myelin as an inflammatory mediator: Myelin interactions with complement, macrophages, and microglia in spinal cord injury. J Neurosci Res. 96, 969–977. [PubMed: 28696010]

Kopper TJ, et al. , 2021. The effects of myelin on macrophage activation are phenotypic specific via cPLA2 in the context of spinal cord injury inflammation. Sci Rep. 11, 6341. [PubMed: 33737707]

Kroner A, et al. , 2014. TNF and increased intracellular iron alter macrophage polarization to a detrimental M1 phenotype in the injured spinal cord. Neuron. 83, 1098–116. [PubMed: 25132469]

Larocca JN, Norton WT, 2007. Isolation of myelin. Curr Protoc Cell Biol. Chapter 3, Unit3 25. [PubMed: 18228513]

Lilley E, et al. , 2020. Refining rodent models of spinal cord injury. Exp Neurol. 328, 113273. [PubMed: 32142803]

Liu Y, et al. , 2006. Suppression of microglial inflammatory activity by myelin phagocytosis: role of p47-PHOX-mediated generation of reactive oxygen species. J Neurosci. 26, 12904–13. [PubMed: 17167081]

Matthieu JM, et al. , 1981. Similarities and dissimilarities between two myelin deficient mutant mice, Shiverer and mld. Brain Res. 214, 219–22. [PubMed: 6165444]

Milich LM, et al. , 2021. Single-cell analysis of the cellular heterogeneity and interactions in the injured mouse spinal cord. J Exp Med. 218.

Milich LM, et al. , 2019. The origin, fate, and contribution of macrophages to spinal cord injury pathology. Acta Neuropathol. 137, 785–797. [PubMed: 30929040]

Myers SA, et al. , 2014. CD36 deletion improves recovery from spinal cord injury. Exp Neurol. 256, 25–38. [PubMed: 24690303]

Nagaike K, et al. , 1982. Dysmyelination of shiverer mutant mice in vivo and in vitro. J Neurochem. 39, 1235–41. [PubMed: 6750046]

Nguyen MA, et al. , 2018. Extracellular Vesicles Secreted by Atherogenic Macrophages Transfer MicroRNA to Inhibit Cell Migration. Arterioscler Thromb Vasc Biol. 38, 49–63. [PubMed: 28882869]

Perrin FE, et al. , 2005. Involvement of monocyte chemoattractant protein-1, macrophage inflammatory protein-1alpha and interleukin-1beta in Wallerian degeneration. Brain. 128, 854–66. [PubMed: 15689362]

Popovich PG, et al. , 1999. Depletion of hematogenous macrophages promotes partial hindlimb recovery and neuroanatomical repair after experimental spinal cord injury. Exp Neurol. 158, 351–65. [PubMed: 10415142]

Ren Y, et al. , 2001. Nonphlogistic clearance of late apoptotic neutrophils by macrophages: efficient phagocytosis independent of beta 2 integrins. J Immunol. 166, 4743–50. [PubMed: 11254736]

Ren Y, Young W, 2013. Managing inflammation after spinal cord injury through manipulation of macrophage function. Neural Plast. 2013, 945034. [PubMed: 24288627]

Rumsby MG, et al. , 1970. A critical evaluation of myelin purification. Non-specific esterase activity associated with central nerve myelin preparations. Brain Res. 24, 495–516. [PubMed: 5494537]

Siddiqui TA, et al. , 2016. Complex molecular and functional outcomes of single versus sequential cytokine stimulation of rat microglia. J Neuroinflammation. 13, 66. [PubMed: 27009332]

Stewart AN, et al. , 2020. Considerations for Studying Sex as a Biological Variable in Spinal Cord Injury. Front Neurol. 11, 802. [PubMed: 32849242]

Sun X, et al. , 2010. Myelin activates FAK/Akt/NF-kappaB pathways and provokes CR3-dependent inflammatory response in murine system. PLoS One. 5, e9380. [PubMed: 20186338]

Van Broeckhoven J, et al. , 2021. Macrophage phagocytosis after spinal cord injury: when friends become foes. Brain.

van der Laan LJ, et al. , 1996. Macrophage phagocytosis of myelin in vitro determined by flow cytometry: phagocytosis is mediated by CR3 and induces production of tumor necrosis factor-alpha and nitric oxide. J Neuroimmunol. 70, 145–52. [PubMed: 8898723]

van Rossum D, et al. , 2008. Myelin-phagocytosing macrophages in isolated sciatic and optic nerves reveal a unique reactive phenotype. Glia. 56, 271–83. [PubMed: 18069669]

Wang X, et al. , 2015. Macrophages in spinal cord injury: phenotypic and functional change from exposure to myelin debris. Glia. 63, 635–51. [PubMed: 25452166]

Zhou Q, et al. , 2019. Activating Adiponectin Signaling with Exogenous AdipoRon Reduces Myelin Lipid Accumulation and Suppresses Macrophage Recruitment after Spinal Cord Injury. J Neurotrauma. 36, 903–918. [PubMed: 30221582]

Zhu Y, et al. , 2017. Macrophage Transcriptional Profile Identifies Lipid Catabolic Pathways That Can Be Therapeutically Targeted after Spinal Cord Injury. J Neurosci. 37, 2362–2376. [PubMed: 28130359]

Zhu Y, et al. , 2015. Hematogenous macrophage depletion reduces the fibrotic scar and increases axonal growth after spinal cord injury. Neurobiol Dis. 74, 114–25. [PubMed: 25461258]

Highlights

- Development of high content assay for primary foamy macrophages treated with spinal cord homogenate
- Myelin and non-myelin sources of exogenous lipids drive foamy macrophage formation after SCI
- Myelin-deficient mice exhibit decreased lipid content and immune cell infiltration after SCI

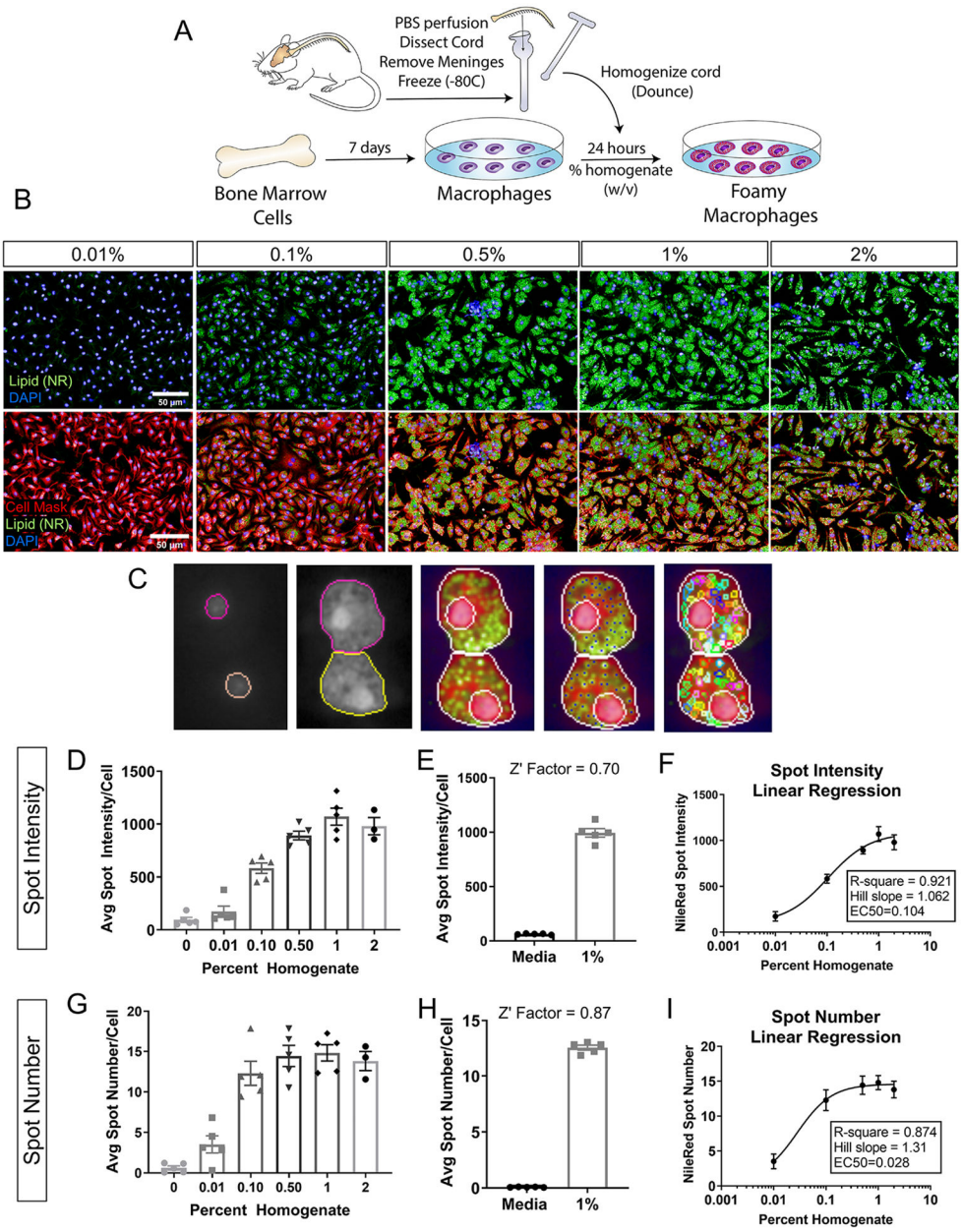

Figure 1. Foamy macrophage assay development and optimization.

(A) Schematic of foamy macrophage assay workflow. (B) Representative images of foamy macrophages treated with wildtype spinal cord homogenate at 0.01, 0.1, 0.5,1.0, and 2.0% (w/v, weight/volume). Neutral lipid droplets stained with Nile Red (green), nuclei with DAPI (blue), cell membrane with Cell Mask (pseudo-colored red) (Scale bar 50 µm). (C) Examples of nuclei and cell segmentation, and lipid droplet identification used in the phenotypic analyses. (D) Dose response for lipid droplet fluorescence intensity in macrophages treated with 0.01, 0.1, 0.5,1.0, and 2.0% homogenate (w/v) (E) Z' factor calculations between positive (1% homogenate) and negative (media only) controls for lipid droplet intensity. (F) 4-parameter nonlinear regression fit of homogenate dose response curve using lipid droplet intensity. x-axis is expressed in logarithmic form. Goodness

of fit assessed by R-square value and linearity of response calculated by Hill's Slope (1.0=perfectly linear). (G) Dose response for lipid droplet number for macrophages treated with 0.01, 0.1, 0.5,1.0, and 2.0% homogenate (w/v). (H) Z' factor calculations between positive (1% homogenate) and negative (media only) controls for lipid droplet number. (I) 4-parameter nonlinear regression fit of homogenate dose response curve using lipid droplet number. x-axis is expressed in logarithmic form. (n=5 biological replicates for 0-1%; n=3 for 2% condition; n=5 technical replicates in E, H; error bars=SEM)

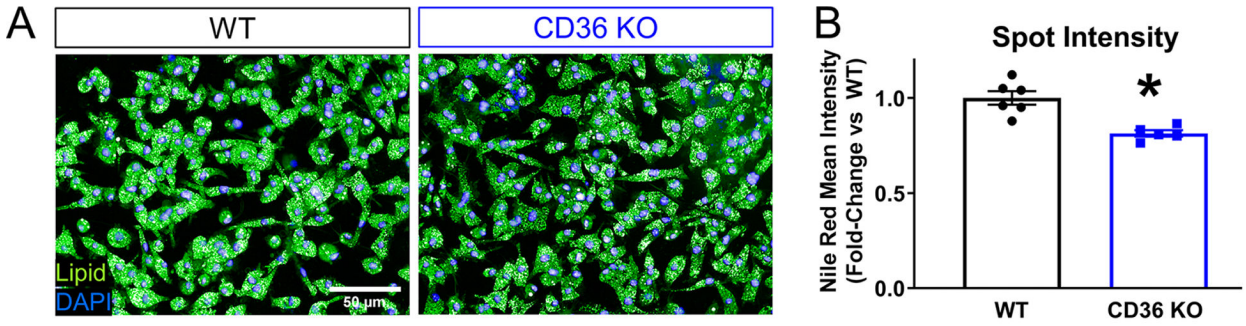

Figure 2. Reduced lipid droplet fluorescence intensity in CD36 KO BMDMs validates foamy macrophage assay.

(A) Representative images from wildtype and CD36 KO macrophages treated with 1% wildtype homogenate. Neutral lipid droplets stained with Nile Red (green) and nuclei with DAPI (blue), scale bar=50 μm. (B) Mean spot intensity per cell in wildtype versus CD36 KO macrophages (n=6 biological replicates in WT, n=5 biological replicates in KO, *p≤0.05 compared to WT, Two-tailed Student's t-test, , error bars=SEM)

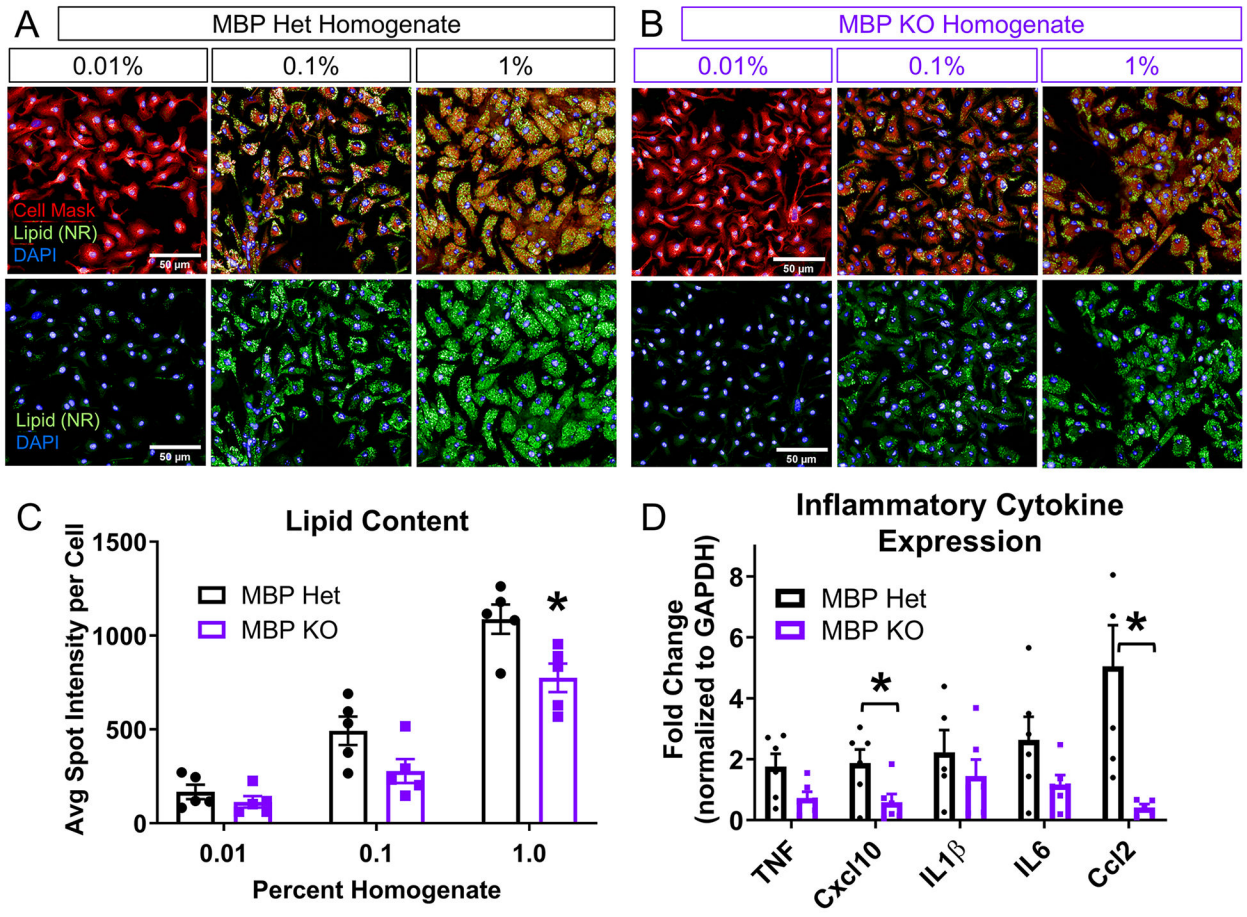

Figure 3. Foamy macrophages can form without myelin *in vitro*.

(A) Representative images from macrophages treated with 0.01, 0.1, and 1.0% (w/v) MBP Het homogenate, which contains normal amount of myelin. Neutral lipid droplets stained with Nile Red (green), cell membrane with Cell Mask (red), and nuclei with DAPI (blue), scale bar=50 µm. (B) Representative images from macrophages treated with 0.01, 0.1, and 1.0% (w/v) MBP KO homogenate, which is deficient in myelin. Neutral lipid droplets stained with Nile Red (green), cell membrane with Cell Mask (red), and nuclei with DAPI (blue), scale bar=50 µm. (C) Measurement of lipid droplet fluorescence demonstrates a concentration-dependent increase in intensity in macrophages after treatment with either MBP Het or KO spinal cord homogenate. Treatment with MBP KO homogenate showed decreased spot intensity compared to Het homogenate at 1% concentration (n=5 biological replicates, Two-way ANOVA with Bonferroni multiple comparisons, *P≤0.05 compared to MBP Het at corresponding concentration, error bars SEM.). (D) qPCR analysis of inflammatory cytokine expression (n=6 biological replicates per group, *p≤0.05 compared to MBP Het, Two-tailed Student's t-test per cytokine, error bars=SEM)

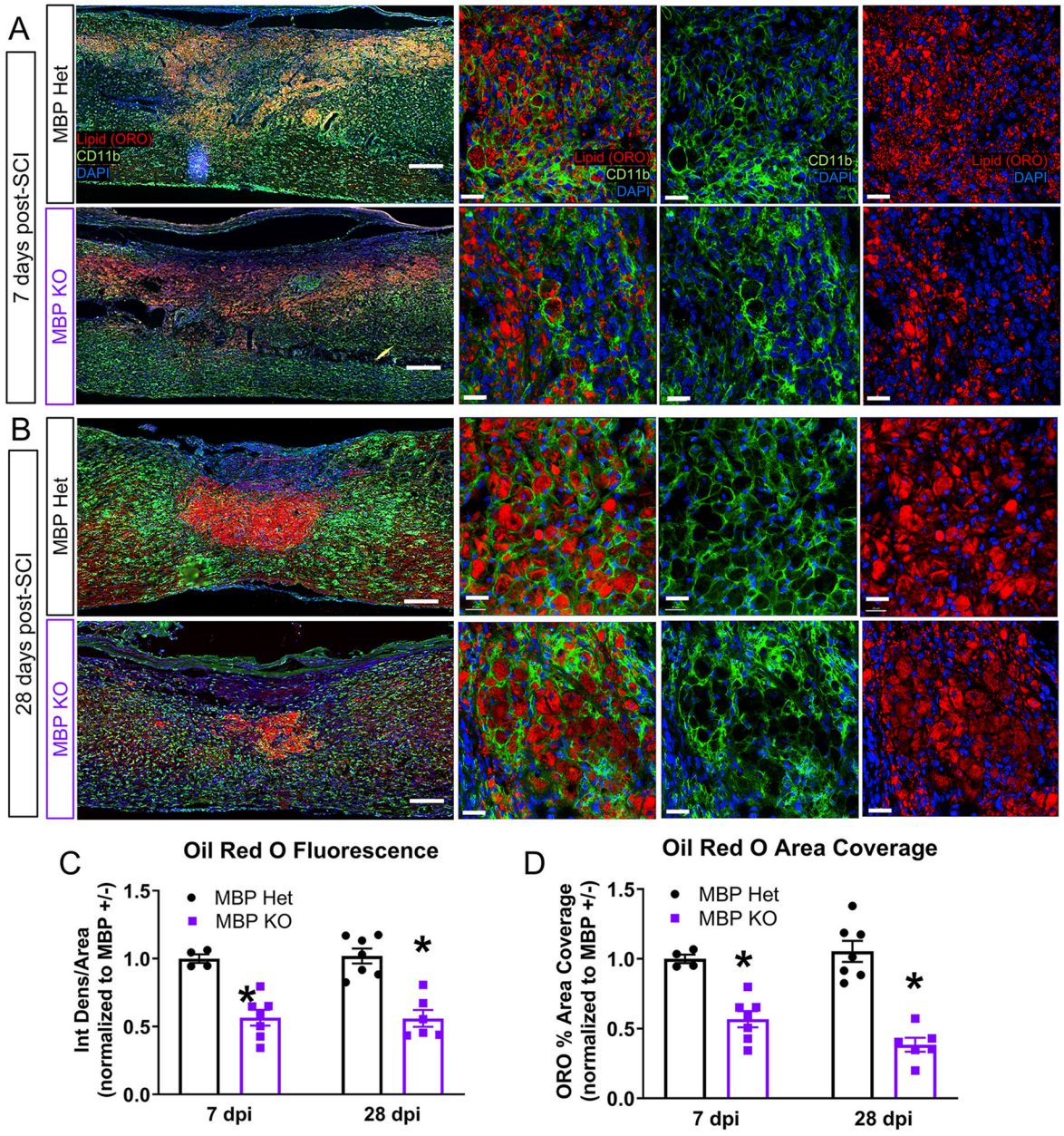

Figure 4. Foamy macrophages can form without myelin in vivo.

(A) Representative images from the injury site in MBP Het and KO mice at 7 days post injury (dpi). Lipid droplets stained with Oil Red O (red), myeloid cells labeled with CD11b (green) and nuclei with DAPI (blue). Scale Bar=200 μm in low magnification images, Scale Bar=50 μm in high magnification images. (B) Representative images from the SCI injury site in MBP Het and KO mice at 28 dpi. (C) Quantification of Oil Red O lipid droplet fluorescence in MBP KO and Het injury sites at 7 and 28 dpi (7 dpi: MBP Het n=4, MBP KO n=7, 28 dpi: MBP Het n=7, MBP KO n=6, n represents biological replicates, *p≤0.05 compared to Het, Two-tailed Student's t-test per time point, error bars=SEM). (D) Quantification of Oil Red O lipid droplet area coverage in MBP KO and Het injury sites at 7 and 28 dpi (biological replicates and statistics same as in (C))

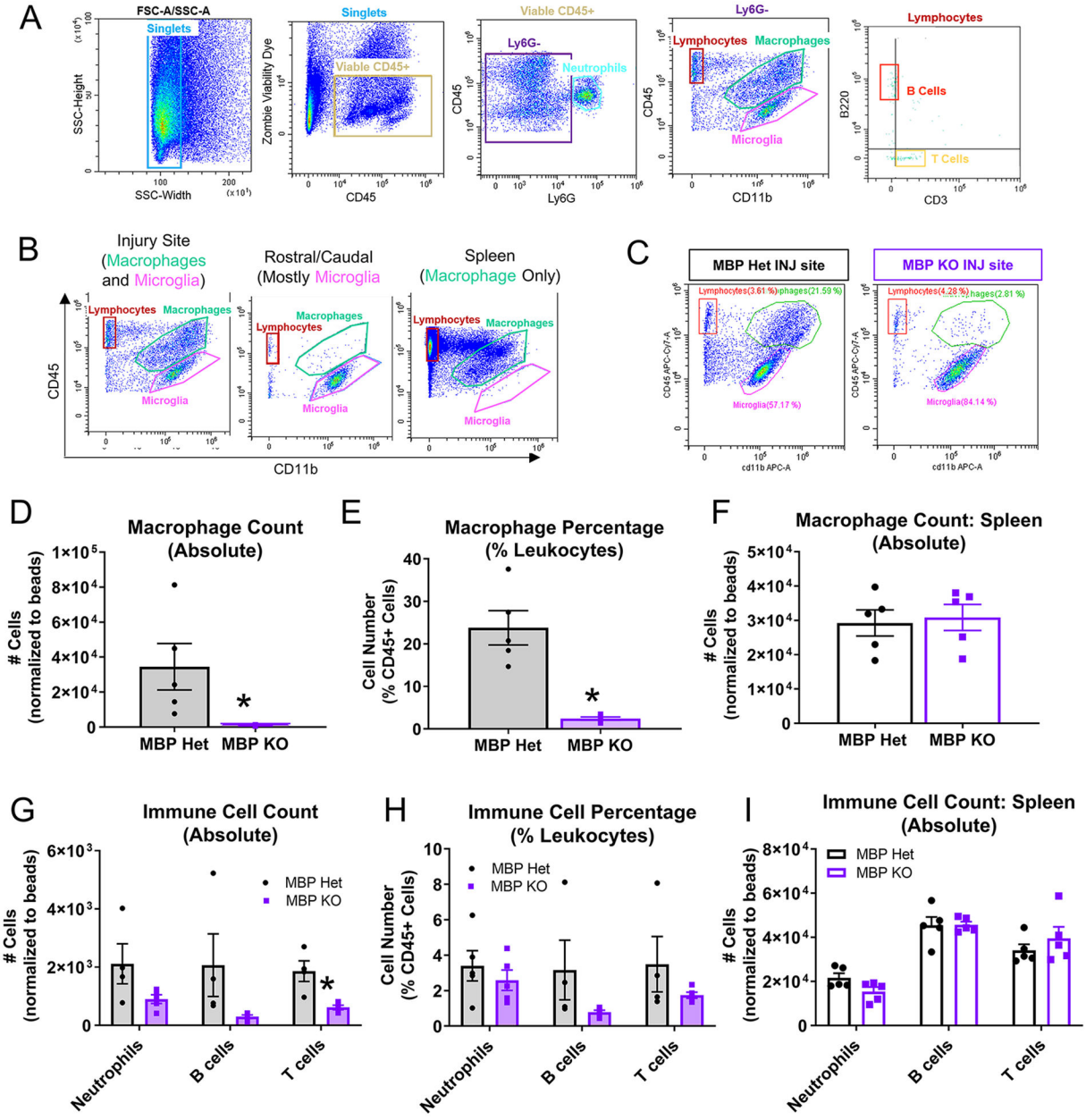

Figure 5. Reduced leukocyte infiltration in MBP KO mice at 7 dpi.

(A) Gating strategy for immune cell flow analysis: viable CD45+ singlets were separated by Ly6G expression to identify neutrophils ($Ly6G^+/CD45^+$). $Ly6G^-CD45^+$ cells were separated by CD45 and CD11b expression to distinguish macrophage ($CD11b^+CD45^{hi}$) from microglia ($CD11b^+CD45^{lo}$) populations, and to identify $CD45^+CD11b^-$ lymphocytes. Lymphocytes were separated into $B220^+$ B cells and $CD3^+$ T cells. (B) Spinal cord tissues rostral/caudal to the injury site were used to determine gating for microglia, and spleen was used for gating macrophages. (C) Representative flow plots showing macrophage and microglia populations in the MBP Het versus MBP KO injury site (7 dpi). (D, E) Macrophage number and percentage decreased in MBP KO injury site (n=5 biological replicates per group, *p≤0.05 compared to Het, Two-tailed Student's t-test,

error bars=SEM). (F) Number of splenic macrophages were not different between MBP KO and Het (n=5 biological replicates per group, *p≤0.05 compared to Het, Two-tailed Student's t-test, error bars=SEM). (G, H) Reduced lymphocyte number and percentage in MBP Het injury site (biological replicates and statistics same as in D, E). (I) Number of splenic lymphocytes were not different between MBP KO and Het (biological replicates and statistics same as in F)

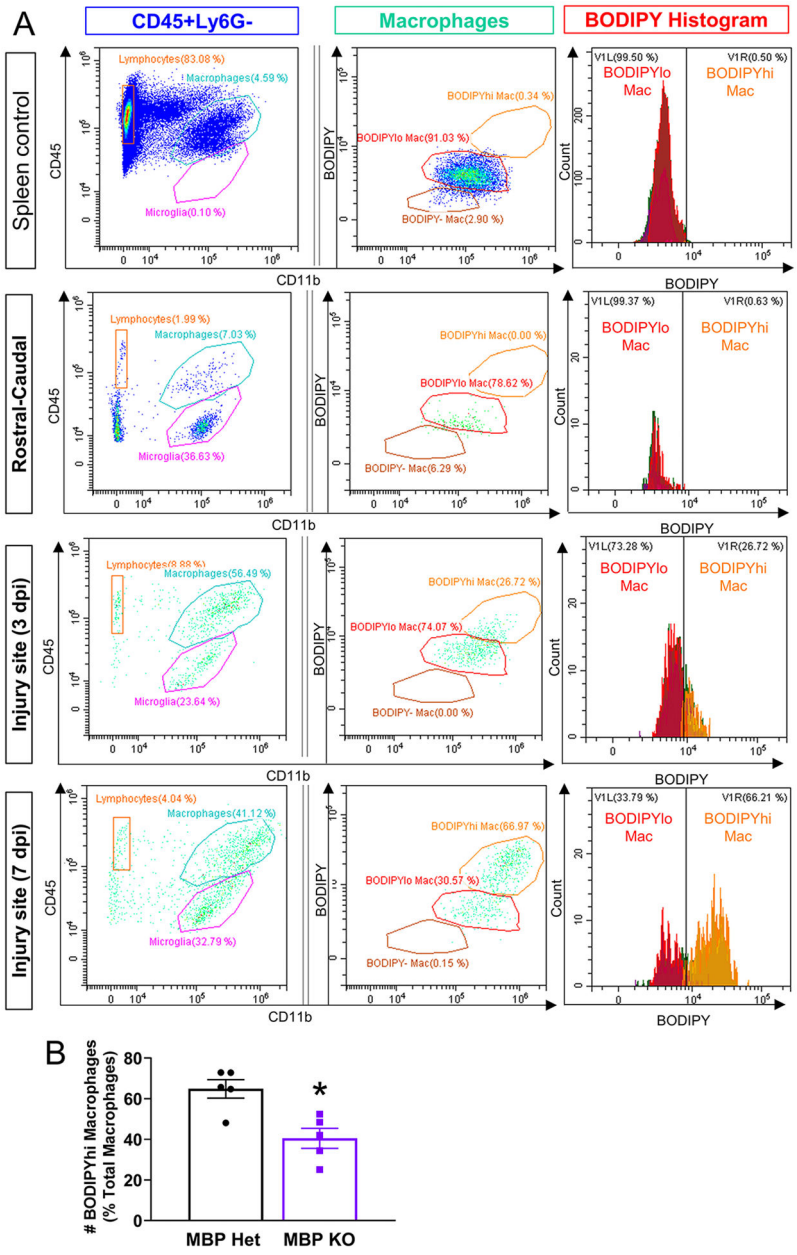

Figure 6. Reduced foamy macrophages in MBP KO injury site at 7 dpi as assessed by flow cytometry.

(A) BODIPY lipid droplet fluorescence in macrophages ($CD11b^{+}CD45^{hi}$) from spleen, spinal cord tissue rostral-caudal to the injury site, and injury sites from 3 and the 7 dpi. $BODIPY^{hi}$ macrophages are present only after SCI, and increases from 3 to 7dpi. (B) Quantification of BODIPY-hi macrophages at 7 dpi expressed as percent of total macrophages.

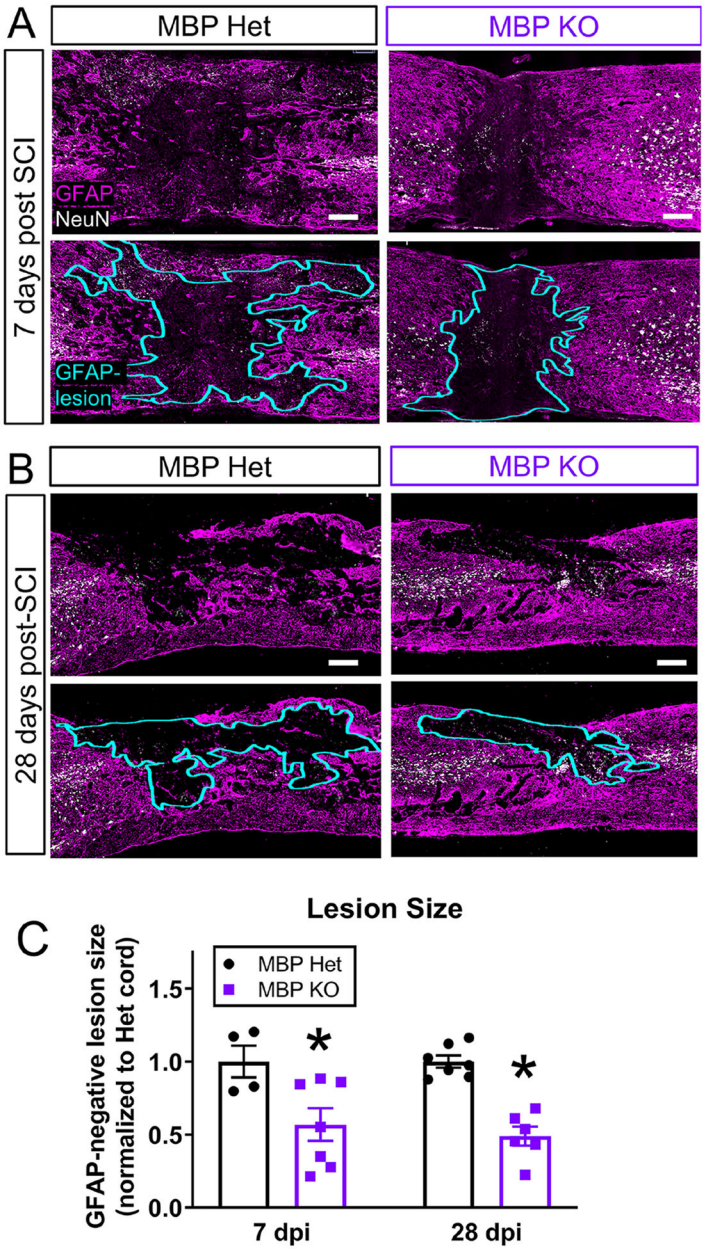

Figure 7. MBP KO mice exhibit decrease in lesion size at 7 and 28 dpi.

(A) Representative images of GFAP-negative lesion sites at 7 dpi in MBP Het and KO mice. GFAP peudo-colored in magenta. NeuN in white. GFAP-negative region outlined in aqua. (B) Representative image of the injury site at 28 dpi. (C) GFAP-negative lesion size was decreased in myelin-deficient MBP mutants compared to MBP Het controls at 7 and 28 dpi (7 dpi: MBP Het n=4, MBP KO n=7, 28 dpi: MBP Het n=7, MBP KO n=6, n=biological replicates, *p≤0.05 compared to Het, Two-tailed Student's t-test per time point, , error bars=SEM)

Table 1:

qPCR primer sequences

Gene	Forward Primer (5'→3')	Reverse Primer (5'→3')
Tnf	AGGCACTCCCCCAAAAGATG	TCACCCCGAAGTTCAGTAGAC
Il-1β	CTTCAAATCTCACAGCAGCAGCACATC	CCACGGGAAAGACACAGGTAG
Il-6	AACCACGGCCTTCCCTACTTCA	TCATTTCCACGATTTCCCAGAG
Cxcl10	GCCGTCATTTTCTGCCTCATCCT	CTCATTCTCACTGGCCCGTCATC
Ccl2	TGCCCACGTCAAGGAGTATTTCTA	CCTGCTGCTGGTGATTCTCTT
Gapdh	TGGCCTTCCGTGTTCCTAC	GAGTTGCTGTTGAAGTCG